Original Article | Nuclear Medicine

eISSN 2005-8330
https://doi.org/10.3348/kjr.2022.0320
Korean J Radiol 2022;23(10):986-997

Korean Journal of Radiology
KJR

Brain Metabolic Network Redistribution in Patients with White Matter Hyperintensities on MRI Analyzed with an Individualized Index Derived from ^{18}F-FDG-PET/MRI

Jie Ma[1, 2*], Xu-Yun Hua[3*], Mou-Xiong Zheng[3], Jia-Jia Wu[1], Bei-Bei Huo[2], Xiang-Xin Xing[1], Xin Gao[4], Han Zhang[5], Jian-Guang Xu[1, 2, 6]

[1]Center of Rehabilitation Medicine, Yueyang Hospital of Integrated Traditional Chinese and Western Medicine, Shanghai University of Traditional Chinese Medicine, Shanghai, China; [2]School of Rehabilitation Science, Shanghai University of Traditional Chinese Medicine, Shanghai, China; [3]Department of Traumatology and Orthopedics, Yueyang Hospital of Integrated Traditional Chinese and Western Medicine, Shanghai University of Traditional Chinese Medicine, Shanghai, China; [4]Panoramic Medical Imaging Diagnostic Center, Shanghai, China; [5]School of Biomedical Engineering, ShanghaiTech University, Shanghai, China; [6]Engineering Research Center of Traditional Chinese Medicine Intelligent Rehabilitation, Ministry of Education, Shanghai, China

Objective: Whether metabolic redistribution occurs in patients with white matter hyperintensities (WMHs) on magnetic resonance imaging (MRI) is unknown. This study aimed 1) to propose a measure of the brain metabolic network for an individual patient and preliminarily apply it to identify impaired metabolic networks in patients with WMHs, and 2) to explore the clinical and imaging features of metabolic redistribution in patients with WMHs.

Materials and Methods: This study included 50 patients with WMHs and 70 healthy controls (HCs) who underwent ^{18}F-fluorodeoxyglucose-positron emission tomography/MRI. Various global property parameters according to graph theory and an individual parameter of brain metabolic network called "individual contribution index" were obtained. Parameter values were compared between the WMH and HC groups. The performance of the parameters in discriminating between the two groups was assessed using the area under the receiver operating characteristic curve (AUC). The correlation between the individual contribution index and Fazekas score was assessed, and the interaction between age and individual contribution index was determined. A generalized linear model was fitted with the individual contribution index as the dependent variable and the mean standardized uptake value (SUV_{mean}) of nodes in the whole-brain network or seven classic functional networks as independent variables to determine their association.

Results: The means ± standard deviations of the individual contribution index were (0.697 ± 10.9) x 10^{-3} and (0.0967 ± 0.0545) x 10^{-3} in the WMH and HC groups, respectively ($p < 0.001$). The AUC of the individual contribution index was 0.864 (95% confidence interval, 0.785–0.943). A positive correlation was identified between the individual contribution index and the Fazekas scores in patients with WMHs ($r = 0.57$, $p < 0.001$). Age and individual contribution index demonstrated a significant interaction effect on the Fazekas score. A significant direct association was observed between the individual contribution index and the SUV_{mean} of the limbic network ($p < 0.001$).

Conclusion: The individual contribution index may demonstrate the redistribution of the brain metabolic network in patients with WMHs.

Keywords: *White matter hyperintensities; Individual contribution index; Brain metabolic network; Individual-level*

Received: May 18, 2022 **Revised:** August 1, 2022 **Accepted:** August 2, 2022

*These authors contributed equally to this work.

Corresponding author: Jian-Guang Xu, MD, PhD, School of Rehabilitation Science, Shanghai University of Traditional Chinese Medicine, No. 1200 Cailun Road, Zhangjiang High-tech Park, Pudong New District, Shanghai 201203, China.
• E-mail: xjg@shutcm.edu.cn; and
Han Zhang, PhD, School of Biomedical Engineering, ShanghaiTech University, No. 393 Huaxia Middle Road, Pudong New District, Shanghai 201210, China.
• E-mail: zhanghan2@shanghaitech.edu.cn

Korean Journal of Radiology
KJR

INTRODUCTION

White matter hyperintensities (WMHs) on magnetic resonance imaging (MRI) are very common presentations in brain imaging. Many studies have demonstrated that severe WMHs are strongly associated with stroke, cognitive decline, and gait instability, and abnormalities in local brain regions and functional connectivity have been identified in patients with WMHs [1-3]. Accumulating evidence from neuroimaging techniques supports the idea that the brain is a complex network of interconnected areas [4-6]. WMHs are also considered syndromes involving disconnection of brain networks; functional MRI (fMRI) studies on the structural or functional brain support this hypothesis [7,8]. However, whether redistribution of brain metabolic networks occurs in patients with WMHs, especially in patients demonstrating WMHs but without cognitive decline, remains unknown.

Glucose, the main metabolic substrate of the brain, is necessary to produce energy for cerebral activity, with the energy demands of signal transduction and neurotransmission exceeding 80% of the total cerebral energy consumption [9]. Positron emission tomography (PET) is an important technique that can detect physiological metabolic processes using various radioactive ligands [10]. PET offers a unique potential for localizing and quantifying metabolic changes; it can increase diagnostic certainty by reflecting brain functions in typically affected brain regions and is suitable for monitoring disease progression [11]. PET has been gaining increased usage in exploring neural activity in the brain from the perspective of metabolism. Cerebral glucose metabolism is the primary source of energy for neuronal activity and is closely associated with local neural function, density, and integrity. Fluorodeoxyglucose (FDG) PET is the most frequently used in research on brain activity [12,13]. Our previous research revealed the characteristics of disruption and reorganization of metabolic connectivity in patients with WMHs and provided useful information on the neurophysiological mechanisms that may link the development of WMHs to a disabling status. However, some important issues remain unaddressed. The conventional method for metabolic network construction is based on the metabolic covariance within a group of subjects [14]. Only one correlation matrix was acquired for the whole group, and variance information at the individual level was lost [13,15]. Therefore, the relationships between metabolic properties in an individual brain and clinical measures, such as age and disease severity, could not be analyzed. Although many indicators describing brain status in particular diseases have been reported, markers for identifying early metabolic network injury on FDG-PET images are yet to be determined.

Thus, this study aimed 1) to propose a measure of brain metabolic network for an individual patient and preliminarily apply it to identify impaired metabolic networks in patients with WMHs, and 2) to explore the clinical and imaging features of metabolic redistribution in patients with WMHs. To accomplish this, we calculated global network properties based on individual networks, including small-worldness, efficiency, assortativity, synchronization, and hierarchy. An individualized index called the "individual contribution index" was estimated using a leave-one-subject-out method [16].

MATERIALS AND METHODS

Study Population

Whole-body ^{18}F-FDG-PET/MRI images of 120 consecutive participants who visited the Panoramic Medical Imaging Diagnostic Center in Shanghai between January 2017 and December 2019 were retrospectively collected. Of these 120 participants, 50 with WMHs were assigned to the WMH group, and 70 healthy participants were considered the controls (referred to as the HC group). The population was homogeneous in terms of race (Han nationality) and diet (dietary structure based on raw plant materials). This study was approved by the Institutional Review Board of our hospital (IRB No. 2020-188).

Inclusion and Exclusion Criteria

We included participants aged ≥ 18 years who underwent whole-body ^{18}F-FDG-PET/MRI. The WMH group fulfilled the following inclusion criteria: 1) Fazekas score ranging from 1 to 3 according to the MRI presentation [17], 2) modified Rankin Scale (mRS) ≤ 1, 3) no cognitive complaints, and 4) mini-mental state examination (MMSE) score > 24. The HC group fulfilled the following inclusion criteria: 1) no abnormal signal on brain MRI, 2) mRS ≤ 1, 3) no cognitive complaints, and 4) MMSE score > 24.

The exclusion criteria for all participants were: 1) any diseases leading to other intracranial lesions (e.g., stroke and tumor), 2) other neurological diseases (e.g., Alzheimer's disease, Parkinson's disease, or epilepsy), 3) systemic diseases (e.g., cancer, severe abnormal glucose metabolism, serious heart, liver, kidney, blood system diseases, or

 https://doi.org/10.3348/kjr.2022.0320

infectious diseases), and 4) psychiatric diseases (e.g., anxiety, depression, or schizophrenia).

The diagnosis was made independently by two senior neurologists and one senior radiologist with over 10 years of work experience based on their own experience combined with the Siemens PET data post-processing software (molecular imaging nerve).

Evaluation of WMHs on MRI using Fazekas Scores

Two senior neurologists with over 10 years of experience, who were blinded to the clinical and fMRI data, analyzed the MRIs to separately rate WMHs in periventricular and deep white matter regions according to the Fazekas scoring system. Disagreements in the imaging analysis were resolved through the advice of a neuroradiologist. Two experienced neurologists and one neuroradiologist used the Fazekas scoring system.

WMHs were defined as signal abnormalities of variable size in the white matter indicating hyperintensities on T2-weighted images, such as fluid-attenuated inversion recovery and no cavitation (signal different from cerebrospinal fluid) [18]. Paraventricular and deep WMHs were scored separately, according to the Fazekas scoring system. The scores for the two parts were summed to calculate the total score. According to the Fazekas scoring system, paraventricular WMHs were recorded as absent (grade 0), cap-like or pencil-like thin-layer lesions (grade 1), smooth halos (grade 2), or irregular paraventricular hyperintensities extending to the deep white matter (grade 3). Deep WMHs were recorded as absent (grade 0), punctate lesions (grade 1), lesions beginning to demonstrate confluency (bridging) (grade 2), or large confluent lesion (grade 3) (Fig. 1).

Evaluation of the mRS Score

The mRS score used to evaluate neurological functioning was divided into six levels. The key mRS issues were completely asymptomatic (0), able to complete all daily activities (≤ 1), able to live independently (≤ 2), able to walk without assistance (≤ 3), not being able to walk independently and needing help from others but not requiring constant supervision (4), and bedbound and needing continuous attention and care (5) [19].

FDG-PET Image Acquisition and Preprocessing

All scans were performed on an integrated 3T PET/MRI device (mMR Biograph, Siemens Healthcare) with simultaneous registration of the MR and PET images. The PET/MRI operating system used was syngo MRI VB20P (Siemens Healthcare GmbH). The participants were instructed to fast for at least 6 hours prior to undergoing an MRI scan, and their blood glucose levels were measured to ensure the absence of hyperglycemia (> 150 mg/dL) before each scan. Light and sound shielding were applied before and during scanning. The participants were required to close their eyes and remain calm throughout the examination. The acquisition time of the PET/MRI scans was 50 minutes with an injection of 3.7 MBq/kg. ^{18}F-FDG-PET/MRI datasets were acquired in five bed positions from the head to mid-thigh with three-dimensional image reconstruction and Gaussian filtering with 4.0-mm FWHM (slice thickness 2.03 mm; acquisition matrix, 172 x 172; in-plane resolution 4.17 x 4.17 mm). The MR images used for MR-based attenuation correction were acquired with breath-holding using a dual-echo spoiled gradient-echo sequence with Dixon fat and water separation (echo time 1 = 1.23 ms, echo time 2 = 2.46 ms, repetition time = 3.6 ms, and flip angle = 10°).

The ^{18}F-FDG-PET brain images of each participant were preprocessed using Statistical Parametric Mapping 12.0 (SPM12; http://www.fil.ion.ucl.ac.uk/spm/) and GRETNA v2.0 [20], running on a MATLAB 2013b platform. The preprocessing included the following stages: 1) Raw PET brain images were converted to the NIFTI format, 2) The edges were cropped, leaving only the brain intact, 3) The origin was set as the anterior commissure, 4) The T1 image was spatially normalized to the standard Montreal Institute of Neurology space, and transformation parameters were applied to the co-registered PET images for PET spatial normalization, 5) PET images were segmented into 90 regions (without the cerebellum) according to an automated anatomical labeling (AAL) system [21] or seven classic networks based on a study by Yeo et al. [22]. 6) The average standardized uptake value (SUV_{mean}) of each region of interest (ROI) was extracted for the analysis. In each participant, the mean ^{18}F-FDG uptake in the ROIs was regressed against the mean ^{18}F-FDG uptake of the whole brain to correct for variability in injected activity (Fig. 2A) [23].

Construction of an Individual Metabolic Network and Computation of Graph Theory Metrics

Previous group-based metabolic network studies have described the metabolic covariance of a group [24] but lost metabolic information at the individual participant level. Here, an individual's metabolic network was constructed using the Jensen–Shannon divergence similarity estimation

https://doi.org/10.3348/kjr.2022.0320

Korean Journal of Radiology
KJR

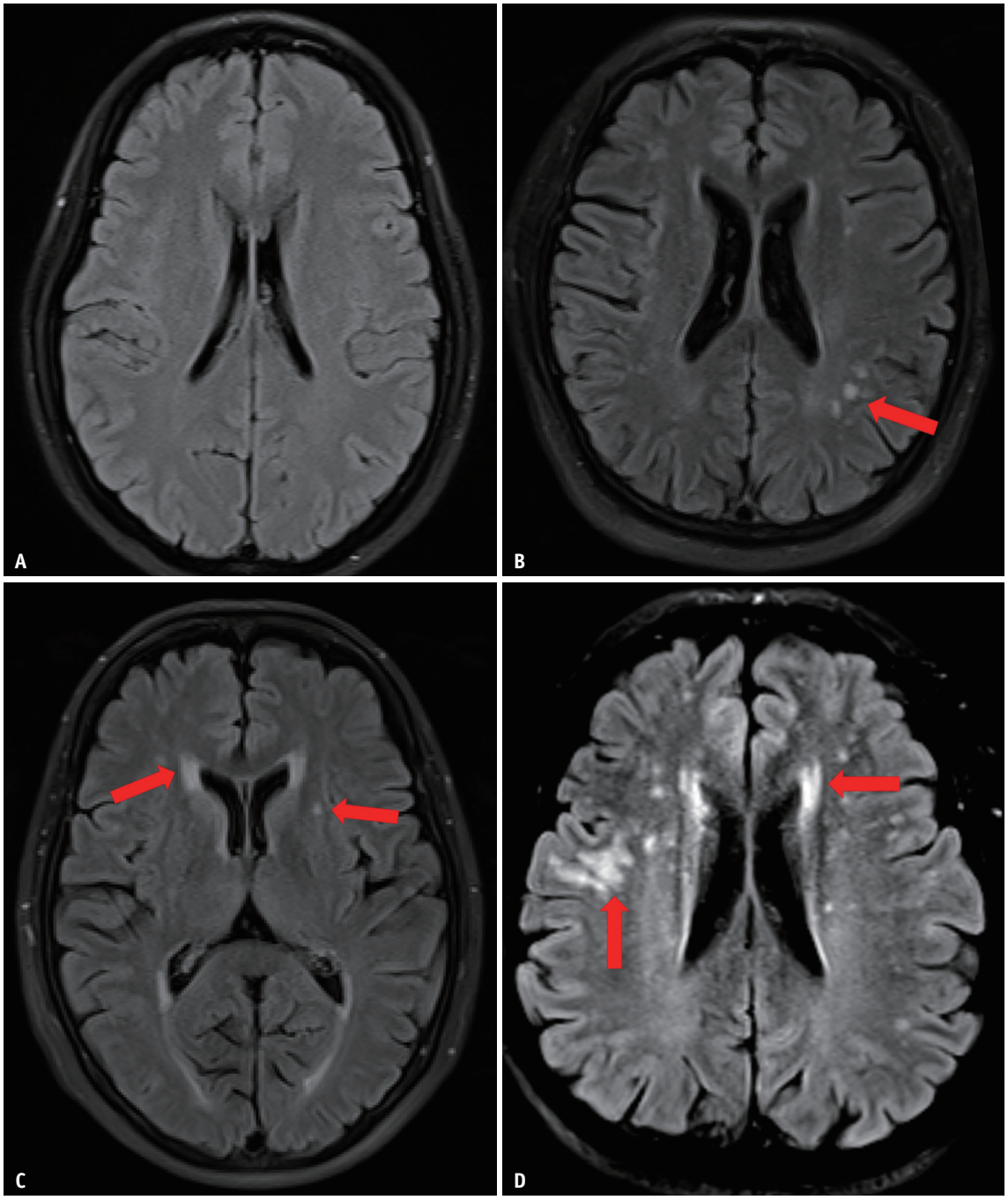

Fig. 1. Demonstration of Fazekas scores on MRI images.
A. No DWM lesions. **B-D.** Arrows represent DWM lesion. Typical DWM lesions with T2-weighted FLAIR hyperintensity. T2-weighted FLAIR hyperintensity in deep white matter **(B)**. T2-weighted FLAIR hyperintensity in both paraventricular and deep white matter (punctate lesions) **(C)**. T2-weighted FLAIR hyperintensity in both paraventricular and deep white matter (patchy lesions) **(D)**. DWM = damaged white matter

(JSSE) method [25]. Ninety ROIs from the AAL atlas were used to represent the nodes. Correlations between each pair of nodes calculated using JSSE describe the similarity of glucose metabolism. The SUV_{mean} of each ROI was extracted to generate a 90 x 90 correlation matrix for each participant [26]. The Jensen–Shannon (JS) divergence was calculated using the following equation:

$$D_{JS}(\mathbf{P}||\mathbf{Q}) = \frac{1}{2}[D_{KL}(\mathbf{P}||\mathbf{M}) + D_{KL}(\mathbf{Q}||\mathbf{M})] \quad (1)$$

where $\mathbf{M}$ = 0.5 x $(\mathbf{P} + \mathbf{Q})$ and $D_{KL}(\cdot \mid \cdot)$ are Kullback–Leibler divergences. The JS divergence is a measure of

 https://doi.org/10.3348/kjr.2022.0320

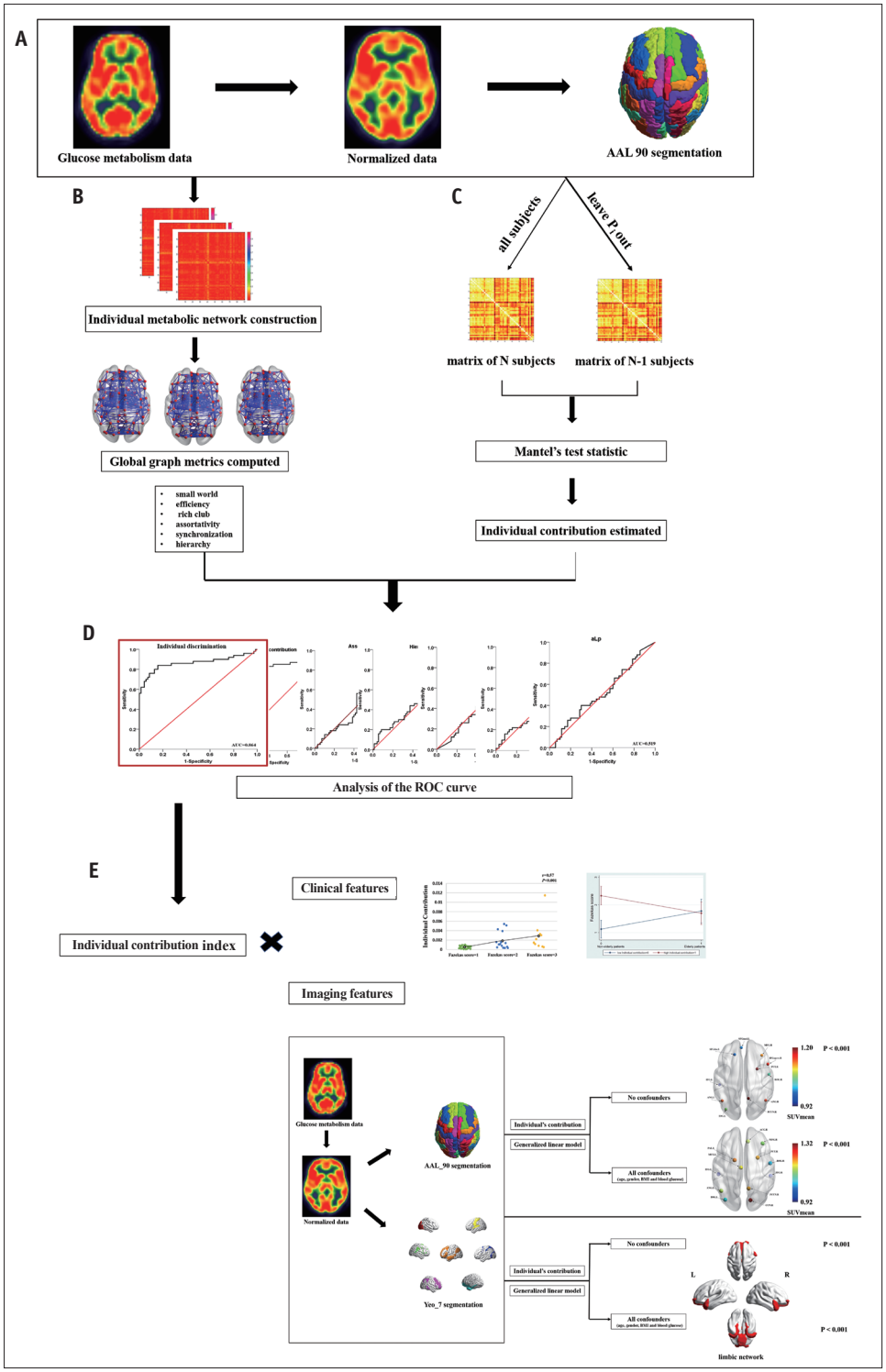

Fig. 2. Flowchart of image preprocessing, construction of individual metabolic networks, calculation of the individual contribution index, and correlation analysis.

A. Image preprocessing and segmentation of each participant. **B.** Construction of individual metabolic networks using the JSSE method. Global graph metrics for each network were then calculated. **C.** Estimation of the contribution of each individual to the overall configuration of the network by extracting the individual contribution index from the overall metabolic correlation matrix. **D.** Analysis of the ROC curve to assess the diagnostic accuracy of the global network parameters and the individual contribution index for distinguishing patients with white matter hyperintensities from participants in the healthy control group. **E.** Analysis of factors associated with the individual contribution index, including clinical features and imaging features. JSSE = Jensen–Shannon Divergence Similarity Estimation, ROC = receiver-operating characteristic

https://doi.org/10.3348/kjr.2022.0320

Korean Journal of Radiology
KJR

metabolic connectivity that is used to construct the adjacency matrix. The global properties of the undirected binary matrices were calculated, including the clustering coefficient (Cp), characteristic path length (Lp), Gamma, Lambda, small-worldness (Sigma), global efficiency (Eglob), local efficiency (Eloc), assortativity, synchronization, and hierarchy (Fig. 2A, B) [20].

Individual Contribution Index

The impact of each individual on the overall group-level configuration of the brain network was measured by extracting the "individual contribution index" from the overall metabolic correlation matrix [16]. In each group, the *P* of each individual was excluded to estimate its contribution to the group [16]. Mantel's test statistic was used to estimate the contribution of each participant according to the similarity between the global correlation matrices before and after leave-one-out. Mantel's test is a method for evaluating the similarity between correlation matrices and can be described as presented in Equation (2) (Fig. 2A, C) [27].

$$Mantel's\ test\ (P,M) = \frac{1}{n-1}\sum_{i=1}^{n}\sum_{j=1}^{n}\frac{P_{ij}-\bar{p}}{S_p}\bullet\frac{m_{ij}-\bar{m}}{S_m} \quad (2)$$

where *n* is the number of elements, and *Sp* and *Sm* are the standard variances of the matrices *P* and *M*, respectively. The Mantel's test coefficient ranges from -1 to 1. A value of 0 indicates no significant difference, and ± 1 represents the maximum positive or negative correlation between matrix *P* and matrix *M*.

The Saggar formula was used to format the individual contribution index of individual *Rx* in the group-level metabolic brain network, using Equation (3).

$$LOO_{Rx} = 1 - Mantel's\ test\ (P_{i=1\ldots n}, P_{i=1\ldots x,x+1\ldots n}) \quad (3)$$

We defined the number of participants in the group as N, then removed one participant and updated the number of participants to N - 1. The individual contribution index was calculated using the Mantel's test. P_i = 1.... N represents continuous removal of P_i from the original group.

Statistical Analysis

For between-group comparisons, the two-sample *t* test was used for continuous variables, and the χ^2 test was used for categorical variables.

Receiver operating characteristic (ROC) curve analysis was conducted to assess the performance of the global property parameters according to graph theory and the individual contribution index to distinguish patients with WMHs from the HC group. Discrimination performance was measured using the area under the ROC curve (AUC). The bootstrap bias-corrected 95% confidence interval (CI) of the AUC was calculated.

Correlation analysis was performed to investigate associations between the Fazekas scores and individual contribution index as well as between the global property parameters and individual contribution index. The joint effect of age and individual contribution index on the Fazekas score was assessed using interaction models with the Fazekas score as the dependent variable. A generalized linear model was fitted to assess the independent association between the SUV_{mean} of the nodes in the whole-brain network, seven classic functional networks, and the individual contribution index (as the dependent variable).

SPSS 21.0 (IBM Corp.) and STATA 16.0 (Stata Corp.), were used for statistical analyses. A two-tailed $p < 0.05$ was considered statistically significant.

RESULTS

Demographics

In total, 120 participants were included in the study. Of the participants, 50 were in the WMH group, and 70 were in the HC group. No significant differences in sex, mean age, body mass index (BMI), and blood glucose were observed between the two groups. The Fazekas scores were grade 1 in 24 (48%), grade 2 in 16 (32%), and grade 3 in 10 individuals (20%) (Table 1).

Global Property Parameters

No significant differences in global network properties

Table 1. Demographics of Patients with WMHs and HC

	WMH Group (n = 50)	HC Group (n = 70)	*P*
Age, year	56.30 ± 9.52	55.49 ± 3.97	0.523
Female	17 (34)	17 (24.3)	0.314
Body mass index, kg/m^2	24.86 ± 3.76	24.07 ± 3.23	0.224
Blood glucose, mmol/L	6.03 ± 1.84	6.06 ± 1.20	0.896
Fazekas score = 1	24 (48)		
Fazekas score = 2	16 (32)		
Fazekas score = 3	10 (20)		

Data are mean ± standard deviation or patient number (%). HC = healthy control, WMHs = white matter hyperintensities

https://doi.org/10.3348/kjr.2022.0320

including Cp, Lp, Gamma, Lambda, Sigma, Eglob, Eloc, assortativity, synchronization, and hierarchy were observed between the two groups (Table 2).

Individual Contribution Index

The mean score ± standard deviation of the individual contribution index was (0.697 ± 10.9) x 10^{-3} in the WMH group and (0.0967 ± 0.0545) x 10^{-3} in the HC group (p < 0.001). The performance of the index in discriminating the WMH and HC groups in terms of AUC was 0.864 (95% CI, 0.785–0.943; p < 0.001) (Fig. 3). The global property parameters exhibited no discrimination capability (Supplementary Fig. 1). Furthermore, according to the correlation analysis between the global property parameters and the individual contribution index, only Lambda demonstrated a weak negative correlation with the individual contribution index (r = -0.191, p = 0.037) (Fig. 4).

Effects of Age and the Individual Contribution Index on Fazekas Scores

A positive correlation was identified between the individual contribution index and the Fazekas score in the WMH group (r = 0.57, p < 0.001) (Fig. 5A). To further explore the effect of the potential interaction between age and the individual contribution index on the Fazekas score, the WMH group was categorized into 2 x 2 subgroups according to age (≥ 60 vs. < 60 years) and the individual

Table 2. Global Property Parameters of Patients with WMHs and HC

	WMH Group (n = 50)	HC Group (n = 70)	*P*
Cp	0.153 ± 0.015	0.152 ± 0.015	0.830
Lp	0.464 ± 0.001	0.464 ± 0.001	0.889
Gamma	0.214 ± 0.014	0.213 ± 0.014	0.651
Lambda	0.300 ± 0.001	0.300 ± 0.001	0.143
Sigma	0.214 ± 0.014	0.213 ± 0.015	0.645
Eglob	0.195 ± 0.001	0.195 ± 0.001	0.869
Eloc	0.223 ± 0.011	0.222 ± 0.011	0.844
Assortativity	-6.820 ± 1.021	-6.938 ± 1.140	0.561
Synchronization	0.161 ± 0.091	0.159 ± 0.109	0.918
Hierarchy	1.631 ± 0.883	1.497 ± 0.883	0.415

Data are mean ± standard deviation. Cp = clustering coefficient, Eglob = global efficiency, Eloc = local efficiency, Gamma = normalized clustering coefficient, HC = healthy control, Lambda = normalized characteristic path length, Lp = characteristic path length, WMHs = white matter hyperintensities

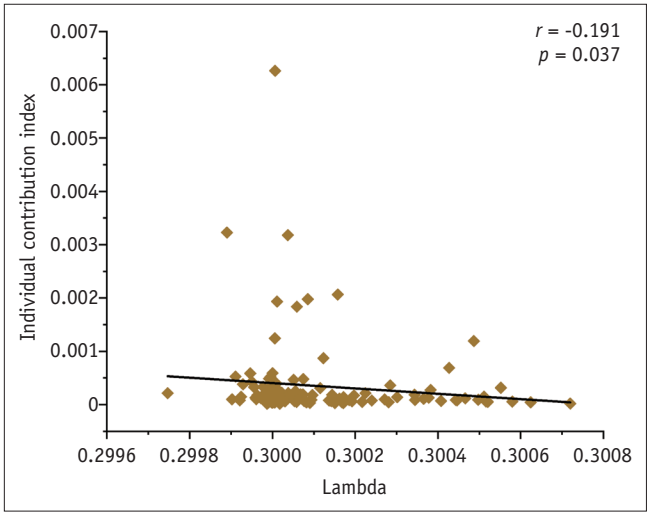

Fig. 4. Scatter plot of Lambda and the individual contribution index, indicating a weak negative correlation.

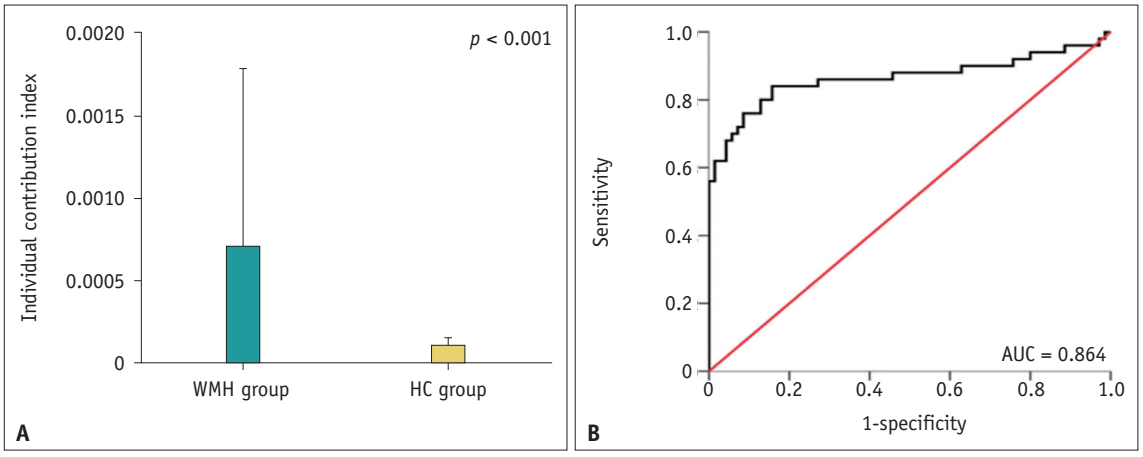

Fig. 3. Individual contribution index values in the WMH and HC groups.
A. A significant difference was observed in the individual contribution index between the WMH and HC groups. **B.** The AUC for discriminating between the two groups was 0.864 (95% confidence interval, 0.785–0.943; p < 0.001). AUC = area under the receiver-operating characteristic curve, HC = healthy control, WMH = white matter hyperintensities

https://doi.org/10.3348/kjr.2022.0320

Korean Journal of Radiology
KJR

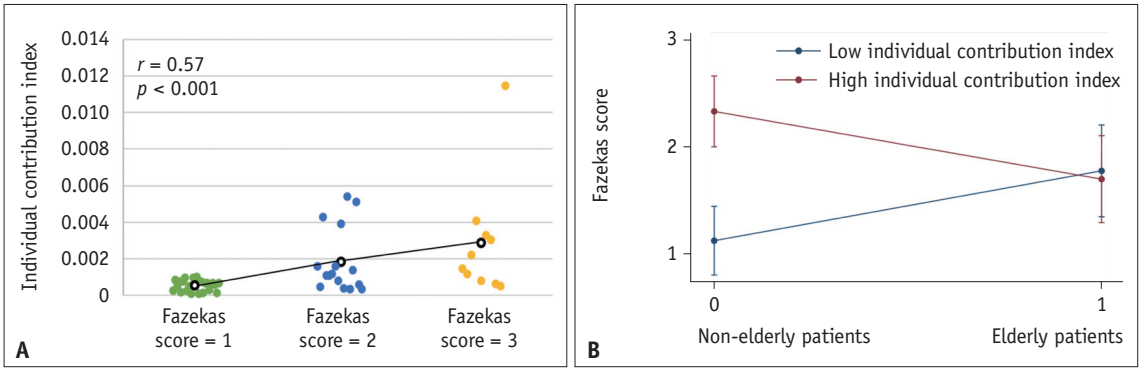

Fig. 5. The effects of age and the individual contribution index on Fazekas scores.
A. Correlation between the individual contribution index and Fazekas score. A positive correlation was identified between the individual contribution index and Fazekas score in participants with WMHs (r = 0.57, p < 0.001). **B.** Predictive marginal means of the Fazekas score with participants stratified by age and the individual contribution index. The confidence intervals of the margins of the Fazekas scores overlapped when the elderly participants were compared across low and high individual contribution index scores. A significant difference was observed when the non-elderly participants were compared across different individual contribution index.

contribution index (high vs. low). The interaction models were fitted using the Fazekas scores as the dependent variable. A significant interaction was observed for this association (β, -1.286 for the interaction term; 95% CI, -2.036 to -0.537; p = 0.001) (Fig. 5B).

To better understand the interaction of non-elderly participants on the association between the individual contribution index and Fazekas scores, we assessed the differences in the predictive marginal means of the Fazekas scores with participants stratified into non-elderly and elderly participants and the individual contribution index. The CIs of the margins of the Fazekas scores overlapped when elderly participants were compared across categories of low and high individual contribution index scores (Fig. 5B). A significant difference was noted when non-elderly participants with WMHs were compared across categories of low and high individual contribution index scores. When elderly participants with WMHs were used as the reference, the β value was 0.633 (95% CI, 0.109–1.158; p = 0.019) (Fig. 5B).

Correlation between Glucose Uptake and the Individual Contribution Index

To investigate the correlation between glucose uptake in each ROI and individual contribution index, a generalized linear model was fitted with the individual contribution index as the dependent variable and the SUV_{mean} of 90 nodes as independent variables. Significant correlations were identified between the individual contribution index and the SUV_{mean} of the left angular gyrus, left inferior temporal gyrus, right precuneus, right angular gyrus, left dorsolateral superior frontal gyrus, left inferior occipital gyrus, left medial superior frontal gyrus, right middle frontal gyrus, right Rolandic operculum, right inferior frontal gyrus (opercular part), and right putamen (p < 0.001). In another generalized linear model with all confounders included (age, sex, BMI, and blood glucose), significant correlations were identified between the individual contribution index and the SUV_{mean} of the left inferior temporal gyrus, right putamen, right precuneus, right middle frontal gyrus, left angular gyrus, right cuneus, right Rolandic operculum, left pallidum, left inferior occipital gyrus, right anterior cingulate gyrus, left median cingulate gyrus, and right inferior temporal gyrus (p < 0.001). In this model, age was a significant variable (p < 0.001) (Fig. 6).

Correlation between Glucose Uptake in the Functional Network and the Individual Contribution Index

To investigate correlations between the individual contribution index and glucose uptake of functional networks, a generalized linear model was fitted with the individual contribution index as the dependent variable and the SUV_{mean} of seven functional networks (visual, somatomotor, dorsal attention, ventral attention, limbic, frontoparietal, and default networks) as independent variables. A significant correlation was identified between the individual contribution index and the SUV_{mean} of the limbic network (β, 0.913; 95% CI, 1.58–3.93; p < 0.001). In another generalized linear model with all confounders included (age, sex, BMI, and blood glucose), a significant correlation was identified between the SUV_{mean} of the limbic network and the individual contribution index (β,

 https://doi.org/10.3348/kjr.2022.0320

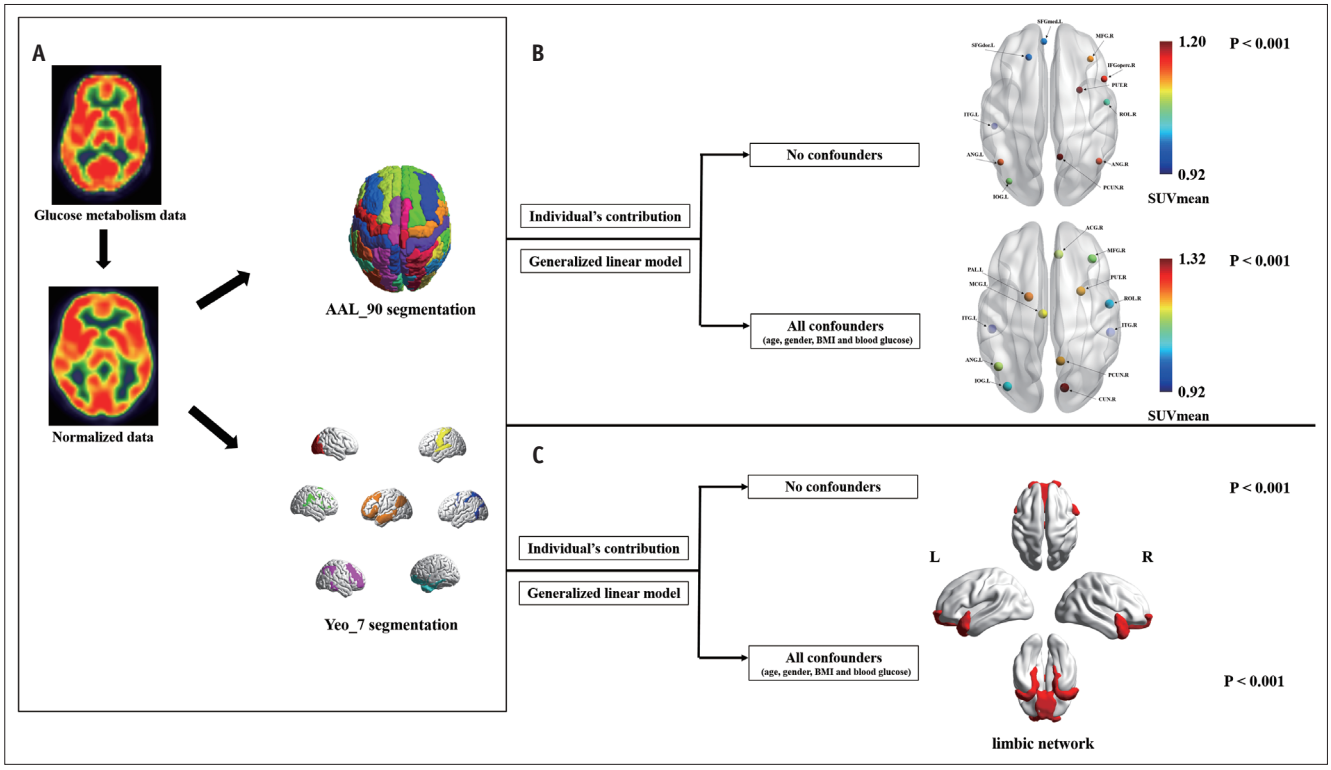

Fig. 6. Correlation between glucose uptake of the functional network and the individual contribution index.
A. Image preprocessing and region of interest segmentation. **B.** A generalized linear model was fitted with the individual contribution index as the dependent variable and all 90 nodes as independent variables with or without confounders. **C.** A generalized linear model was fitted with the individual contribution index as the dependent variable and all seven functional networks (visual, somatomotor, dorsal attention, ventral attention, limbic, frontoparietal, and default network) as independent variables, with or without confounders. BMI = body mass index, SUV_{mean} = mean standardized uptake value

0.953; 95% CI, 1.57–4.28; $p < 0.001$). In this model, all confounders were non-significant variables (Fig. 6).

DISCUSSION

Here, comparisons of global network metrics based on individual metabolic brain networks provided no crucial information regarding differences in abnormal metabolic networks between participants with WMHs (whose Fazekas scores ranged from 1 to 3) and healthy participants. We then used the individual contribution index, which has been widely used in brain network research on nervous system diseases, including studies on metabolic brain networks [16]. The present study investigated the individual contribution index as a method for identifying metabolic brain network damage and its related factors in participants with WMHs to obtain more information and a better understanding of the underlying characteristics of related diseases. The primary findings indicated that the individual contribution index could distinguish the damage to the metabolic network in participants with WMHs. Moreover, associations between the Fazekas score and the SUV_{mean} of the limbic network were identified.

The individual contribution index is estimated based on the leave-one-subject-out strategy, in that an individual is eliminated and the metabolic correlation network is re-estimated at the group level. Similar methods have been used for cross-validation in machine learning [28,29]. Here, the WMH group had a higher individual contribution index than the HC group did, which suggests that participants with a greater individual contribution index may experience more severe damage in the metabolic brain network. Specifically, participants with WMHs and high Fazekas scores sustained more severe damage to the metabolic brain network. Therefore, participants with WMHs and a higher individual contribution index demonstrated worse metabolic network structures. The basic circuit for information communication among subnetworks may be interrupted. Using the leave-one-subject-out approach, Saggar et al. [16] observed lower intelligence scores in individuals with fragile X syndrome who had a higher individual contribution index. This result was consistent with our findings. If the

https://doi.org/10.3348/kjr.2022.0320

Korean Journal of Radiology
KJR

individual contribution index can reflect the optimal balance between individuals and groups, it can be considered a new network parameter for neurophysiological diseases. Additionally, one of the global network parameters, Lambda, demonstrated a negative correlation with the individual contribution index. Lambda is an integration indicator that reflects the brain's ability to gather information from distributed brain areas [30]. Hence, participants with faster information transmission in the glucose metabolism network may demonstrate a higher individual contribution.

In general, the impact of WMHs may increase substantially with the growth of the aged population, which is a leading contributor to age-related dysfunction in brain health. Multiple mechanisms may contribute to the age-related destruction of cerebral small vessel function and structure, although the rate of change can be augmented or inhibited by additional factors, including genetics, environment, behavior, diet, and the presence or absence of various diseases [31]. In our study, a correlation between the individual contribution index and the Fazekas score was identified, and this relationship changed after adding age as a factor. A significant association between the individual contribution index and the Fazekas score was observed in non-elderly participants, although no such association was identified in the elderly. Non-elderly participants with WMHs had lower Fazekas scores only in the presence of a low individual contribution index. Our results verified the hypothesis that WMHs reflect not only the disease itself but also the healthy state of microcirculation in relation to age.

Additionally, this study identified that the network nodes that had an impact on the individual contribution index were distributed in the visual, somatomotor, dorsal attention, limbic, frontoparietal, and default networks. Specifically, the inferior occipital gyrus belongs to the visual network; the Rolandic operculum to the somatomotor network; the inferior temporal gyrus to the dorsal attention network; the dorsolateral superior frontal gyrus and putamen to the limbic network; the middle frontal gyrus and inferior frontal gyrus (opercular part) to the frontoparietal network; and the angular gyrus, precuneus, and medial superior frontal gyrus to the default network. Most of these nodes belong to a default network. Further investigation into the functional network and individual contribution index revealed evident differences in the limbic network, which is involved in higher functions of the human brain, such as cognitive processes and emotional regulation [32]. Studies have reported increased glucose metabolism in the limbic network in several other cognitive diseases [33-35].

The clinical and pathophysiological factors of WMHs have been widely studied using group-level analyses; however, individual differences within groups might have been neglected. We used a novel JSSE [25] method to construct an individual-level metabolic brain network and directly estimated the symmetrical metabolic network using ^{18}F-FDG-PET. We calculated common global network parameters, including small-worldness, efficiency, assortativity, synchronization, and hierarchy, which demonstrated no significant difference between the WMH and HC groups. A possible reason may be that our participants with WMHs were in the early stage of the disease, with Fazekas scores between 1 and 3. The global network parameters may not be sensitive to metabolic brain network injuries in such individuals. Moreover, a relatively small sample size might have limited the detection power. Thus, further studies with larger cohorts are required to verify our preliminary findings.

This study had several limitations. First, because our sample size was small and from the same center, the reliability of the results needs to be further confirmed. Second, owing to the small sample size, we could not cross verify our results. Third, the Fazekas score is a subjective grade. If automated WMHs volume quantitative analysis is used in combination, better results may be obtained. Finally, the negative result might be due to the difficulty in obtaining findings with a small number of participants. Moreover, the patients' conditions were mild, so the metabolic changes in the anatomical regions may also be mild, or metabolism in the anatomical regions may be in the compensatory stage.

In conclusion, the current study demonstrated that the individual contribution index may be used to identify an impaired brain metabolic network in patients with WMHs when compared with the general population. The individual contribution index was related to the Fazekas score and the SUV_{mean} of the limbic network. Further studies may provide an opportunity for the individual identification of brain metabolic network injuries.

Supplement

The Supplement is available with this article at https://doi.org/10.3348/kjr.2022.0320.

Availability of Data and Material

The datasets generated or analyzed during the study are

available from the corresponding author on reasonable request.

Conflicts of Interest

The authors have no potential conflicts of interest to disclose.

Author Contributions

Conceptualization: Jian-Guang Xu. Data curation: Jia-Jia Wu, Bei-Bei Huo. Formal analysis: Xu-Yun Hua. Funding acquisition: Jian-Guang Xu, Xu-Yun Hua, Mou-Xiong Zheng. Investigation: Xiang-Xin Xing. Methodology: Han Zhang. Project administration: Jian-Guang Xu. Software: Han Zhang. Supervision: Jian-Guang Xu. Validation: Xin Gao. Visualization: Jie Ma. Writing—original draft: Jie Ma, Xu-Yun Hua. Writing—review & editing: Mou-Xiong Zheng.

ORCID iDs

Jie Ma
https://orcid.org/0000-0003-0451-7923
Xu-Yun Hua
https://orcid.org/0000-0002-2935-7551
Mou-Xiong Zheng
https://orcid.org/0000-0002-9861-6086
Jia-Jia Wu
https://orcid.org/0000-0001-7515-3958
Bei-Bei Huo
https://orcid.org/0000-0002-0780-9596
Xiang-Xin Xing
https://orcid.org/0000-0001-5699-8525
Xin Gao
https://orcid.org/0000-0003-2444-8611
Han Zhang
https://orcid.org/0000-0002-6645-8810
Jian-Guang Xu
https://orcid.org/0000-0002-9091-8151

Funding Statement

This work was supported by the National Key R&D Program of China (Grant No. 2018YFC2001600, and 2018YFC2001604); National Natural Science Foundation of China (Grant No. 82172554, 81802249, 81871836, and 81902301); Shanghai Talent Development Fund (Grant No. 2021074); Shanghai Municipal Commission of Health and Family Planning (Grant No. 2018YQ02); Shanghai Science and Technology Committee (Grant No. 22010504200); Shanghai Rising-Star Program (Grant No. 19QA1409000); Shanghai Youth Top Talent Development Plan; Shanghai "Rising Stars of Medical Talent" Youth Development Program; Program of Shanghai Academic Research Leader (Grant No. 19XD1403600).

Acknowledgments

We thank all contributors and participants for their contribution to this study.

REFERENCES

1. Kim SJ, Lee DK, Jang YK, Jang H, Kim SE, Cho SH, et al. The effects of longitudinal white matter hyperintensity change on cognitive decline and cortical thinning over three years. *J Clin Med* 2020;9:2663
2. Giese AK, Schirmer MD, Dalca AV, Sridharan R, Donahue KL, Nardin M, et al. White matter hyperintensity burden in acute stroke patients differs by ischemic stroke subtype. *Neurology* 2020;95:e79-e88
3. Venkatraman VK, Aizenstein H, Guralnik J, Newman AB, Glynn NW, Taylor C, et al. Executive control function, brain activation and white matter hyperintensities in older adults. *Neuroimage* 2010;49:3436-3442
4. Frey BM, Petersen M, Schlemm E, Mayer C, Hanning U, Engelke K, et al. White matter integrity and structural brain network topology in cerebral small vessel disease: the Hamburg city health study. *Hum Brain Mapp* 2021;42:1406-1415
5. Chen X, Huang L, Ye Q, Yang D, Qin R, Luo C, et al. Disrupted functional and structural connectivity within default mode network contribute to WMH-related cognitive impairment. *Neuroimage Clin* 2019;24:102088
6. Atwi S, Metcalfe AWS, Robertson AD, Rezmovitz J, Anderson ND, MacIntosh BJ. Attention-related brain activation is altered in older adults with white matter hyperintensities using multi-echo fMRI. *Front Neurosci* 2018;12:748
7. Gesierich B, Tuladhar AM, Ter Telgte A, Wiegertjes K, Konieczny MJ, Finsterwalder S, et al. Alterations and test-retest reliability of functional connectivity network measures in cerebral small vessel disease. *Hum Brain Mapp* 2020;41:2629-2641
8. Ter Telgte A, Wiegertjes K, Tuladhar AM, Noz MP, Marques JP, Gesierich B, et al. Investigating the origin and evolution of cerebral small vessel disease: the RUN DMC - InTENse study. *Eur Stroke J* 2018;3:369-378
9. Shulman RG, Rothman DL, Behar KL, Hyder F. Energetic basis of brain activity: implications for neuroimaging. *Trends Neurosci* 2004;27:489-495
10. Evans NR, Tarkin JM, Buscombe JR, Markus HS, Rudd JHF, Warburton EA. PET imaging of the neurovascular interface in cerebrovascular disease. *Nat Rev Neurol* 2017;13:676-688
11. Heiss WD. The additional value of PET in the assessment of cerebral small vessel disease. *J Nucl Med* 2018;59:1660-1664

12. Tomše P, Jensterle L, Grmek M, Zaletel K, Pirtošek Z, Dhawan V, et al. Abnormal metabolic brain network associated with Parkinson's disease: replication on a new European sample. *Neuroradiology* 2017;59:507-515
13. Huang SY, Hsu JL, Lin KJ, Hsiao IT. A novel individual metabolic brain network for 18F-FDG PET imaging. *Front Neurosci* 2020;14:344
14. Xue X, Wu JJ, Huo BB, Xing XX, Ma J, Li YL, et al. Age-related alterations of brain metabolic network based on [18F] FDG-PET of rats. *Aging (Albany NY)* 2022;14:923-942
15. Wang M, Yan Z, Xiao SY, Zuo C, Jiang J. A novel metabolic connectome method to predict progression to mild cognitive impairment. *Behav Neurol* 2020;2020:2825037
16. Saggar M, Hosseini SM, Bruno JL, Quintin EM, Raman MM, Kesler SR, et al. Estimating individual contribution from group-based structural correlation networks. *Neuroimage* 2015;120:274-284
17. Fazekas F, Chawluk JB, Alavi A, Hurtig HI, Zimmerman RA. MR signal abnormalities at 1.5 T in Alzheimer's dementia and normal aging. *AJR Am J Roentgenol* 1987;149:351-356
18. Wardlaw JM, Smith EE, Biessels GJ, Cordonnier C, Fazekas F, Frayne R, et al. Neuroimaging standards for research into small vessel disease and its contribution to ageing and neurodegeneration. *Lancet Neurol* 2013;12:822-838
19. Bruno A, Shah N, Lin C, Close B, Hess DC, Davis K, et al. Improving modified Rankin Scale assessment with a simplified questionnaire. *Stroke* 2010;41:1048-1050
20. Wang J, Wang X, Xia M, Liao X, Evans A, He Y. GRETNA: a graph theoretical network analysis toolbox for imaging connectomics. *Front Hum Neurosci* 2015;9:386
21. Tzourio-Mazoyer N, Landeau B, Papathanassiou D, Crivello F, Etard O, Delcroix N, et al. Automated anatomical labeling of activations in SPM using a macroscopic anatomical parcellation of the MNI MRI single-subject brain. *Neuroimage* 2002;15:273-289
22. Yeo BT, Krienen FM, Sepulcre J, Sabuncu MR, Lashkari D, Hollinshead M, et al. The organization of the human cerebral cortex estimated by intrinsic functional connectivity. *J Neurophysiol* 2011;106:1125-1165
23. Huo BB, Shen J, Hua XY, Zheng MX, Lu YC, Wu JJ, et al. Alteration of metabolic connectivity in a rat model of deafferentation pain: a 18F-FDG PET/CT study. *J Neurosurg* 2019;132:1295-1303
24. Huang SY, Hsu JL, Lin KJ, Liu HL, Wey SP, Hsiao IT. Characteristic patterns of inter- and intra-hemispheric metabolic connectivity in patients with stable and progressive mild cognitive impairment and Alzheimer's disease. *Sci Rep* 2018;8:13807
25. Li W, Tang Y, Wang Z, Hu S, Gao X. The reconfiguration pattern of individual brain metabolic connectome for Parkinson's disease identification. arXiv [Preprint]. 2021 [cited 2021 April 29]. Available at: https://doi.org/10.48550/arXiv.2105.02811
26. Duong T. KS: kernel density estimation and kernel discriminant analysis for multivariate data in R. *J Stat Softw* 2007;21:1-16
27. Mantel N. The detection of disease clustering and a generalized regression approach. *Cancer Res* 1967;27:209-220
28. Tong Y, Huang X, Qi CX, Shen Y. Altered functional connectivity of the primary visual cortex in patients with iridocyclitis and assessment of its predictive value using machine learning. *Front Immunol* 2021;12:660554
29. Mohanty R, Nair VA, Tellapragada N, Williams LM Jr, Kang TJ, Prabhakaran V. Identification of subclinical language deficit using machine learning classification based on poststroke functional connectivity derived from low frequency oscillations. *Brain Connect* 2019;9:194-208
30. Zhang T, Zhang Y, Ren J, Yang C, Zhou H, Li L, et al. Aberrant basal ganglia-thalamo-cortical network topology in juvenile absence epilepsy: a resting-state EEG-fMRI study. *Seizure* 2021;84:78-83
31. De Silva TM, Faraci FM. Contributions of aging to cerebral small vessel disease. *Annu Rev Physiol* 2020;82:275-295
32. Khastkhodaei Z, Muthuraman M, Yang JW, Groppa S, Luhmann HJ. Functional and directed connectivity of the cortico-limbic network in mice in vivo. *Brain Struct Funct* 2021;226:685-700
33. Ballarini T, Iaccarino L, Magnani G, Ayakta N, Miller BL, Jagust WJ, et al. Neuropsychiatric subsyndromes and brain metabolic network dysfunctions in early onset Alzheimer's disease. *Hum Brain Mapp* 2016;37:4234-4247
34. Sala A, Caminiti SP, Iaccarino L, Beretta L, Iannaccone S, Magnani G, et al. Vulnerability of multiple large-scale brain networks in dementia with Lewy bodies. *Hum Brain Mapp* 2019;40:4537-4550
35. Huber M, Beyer L, Prix C, Schönecker S, Palleis C, Rauchmann BS, et al. Metabolic correlates of dopaminergic loss in dementia with Lewy bodies. *Mov Disord* 2020;35:595-605